Chapter 16
Performance of Nd^{3+} As Structural Probe of Rare-Earth Distribution in Transparent Nanostructured Glass-Ceramics

Rolindes Balda, Giulio Gorni, José J. Velázquez, María J. Pascual, Alicia Durán, and Joaquín Fernández

Abstract Nanostructured glass-ceramics obtained by the adequate heat treatment of a Nd^{3+}-doped glass with composition SiO_2-Al_2O_3-Na_2O-LaF_3 have been investigated by several techniques. X-ray diffraction (XRD) and high resolution transmission electron microscopy (HR-TEM) show that the precipitated nanocrystals are LaF_3 with a crystal size between 9 and 13 nm. Furthermore, energy dispersive X-ray (EDX) analysis shows the incorporation of Nd^{3+} ions into the LaF_3 nano-crystals. A detailed optical characterization clearly shows that Nd^{3+} ions in glass-ceramics are incorporated in both crystalline and amorphous phases. Steady-state and time-resolved site-selective laser spectroscopies allow to isolate unambiguously the emission of Nd^{3+} ions in LaF_3 nanocrystals which shows extremely well defined spectra, similar to those obtained for pure LaF_3 crystal.

Keywords Glass-ceramics · Neodymium · Site-selective laser spectroscopy

16.1 Introduction

The search for new rare earth (RE)-doped materials is still a challenge of great interest for a wide range of photonics applications as well as for scientific basic research. For example, fiber lasers and amplifiers emitting at selected wavelengths

R. Balda · J. Fernández
Departamento de Física Aplicada I, Escuela Superior de Ingeniería, Universidad del País Vasco UPV-EHU, Bilbao, Spain

Materials Physics Center CSIC-UPV/EHU, San Sebastián, Spain
e-mail: rolindes.balda@ehu.eus

G. Gorni · J. J. Velázquez · M. J. Pascual · A. Durán
Instituto de Cerámica y Vidrio (CSIC), Madrid, Spain

B. Di Bartolo et al. (eds.), *Quantum Nano-Photonics*, NATO Science for Peace and Security Series B: Physics and Biophysics,
https://doi.org/10.1007/978-94-024-1544-5_16

in the continuous or pulsed time domain are of paramount importance for bioimaging, optical biosensors, light activated therapy, and telecommunications [1–5]. In particular, RE-doped oxyfluoride glass-ceramics containing one or more crystalline phases embedded in the glass matrix, combine the low phonon energy, optical transparency, and RE ions solubility of fluoride crystals with the good mechanical, thermal, and chemical properties of oxide glasses [6, 7].

The first transparent glass-ceramic (TGC) based on aluminosilicate glass doped with Er^{3+} and Yb^{3+} ions was developed by Wang and Ohwaki in 1993 [8]. It was observed that, exciting Yb^{3+} ions at 970 nm, the green-red upconversion emission from Er^{3+} ions was 100 times more intense than observed from fluoride glass, which suggested the segregation of Yb^{3+} and Er^{3+} ions in the $Pb_xCd_{1-x}F_2$ nano-crystals (NCs). Since then, different RE-doped oxyfluoride glass ceramics mainly based on silicate glass matrices and other fluoride crystal phases, such as LaF_3 [9–11], CaF_2 [12, 13], BaF_2 [14, 15], etc. have been proposed as active media for solid state lasers, optical amplifiers, phosphors or to enhance the efficiency of photovoltaic cells [16, 17].

The rare-earth ions, referred to as the lanthanides, comprise the series of elements in the sixth row of the periodic table after lanthanum from cerium to ytterbium. These atoms are usually incorporated in crystalline or amorphous hosts as trivalent ions and occasionally as divalent ions. The optical activity of the RE ions in solids occurs mainly between electronic states within the 4f configuration. These transitions are parity forbidden and may be partially allowed by crystal field interactions mixing states of different parity. The result is that the transitions between 4f states are weak, with oscillator strengths of the order of 10^{-6}, and radiative lifetimes in the micro and miliseconds range. The long lifetime plays an important role in increasing the probability of sequential excitations in the excited states of a single ion as well as in permitting ion-ion interactions in the excited states to allow energy transfer.

Energy levels in rare-earth ions are labeled according to their angular momentum and spin quantum numbers using terms symbols such as $^4I_{11/2}$, or $^4F_{3/2}$. Here the capital letter refers to the total orbital angular momentum of the ion, the superscript is the spin multiplicity, given as $2S + 1$, where S is the total spin angular momentum. The subscript refers to the total angular momentum of the ion and is determined using the Russell-Saunders coupling scheme [18]. These levels represent the energy levels of a free ion. However, when the ion is in a host, electron-host interactions further split these levels into Stark sublevels, due to the effect of the electric field of the matrix (crystal field effect), which is quite small since the 4f orbitals are shielded from the environment by the filled 5 s and 5p sub-shells. Nevertheless, the crystal field (CF) induced by the host is what determines the shape of the absorption and emission spectra of RE ions. When comparing the spectra of RE ions in crystals and glasses, the absorption and emission bands are narrow with well resolved Stark components, even at room temperature, in the case of crystals where RE ions occupy a well defined crystal field site. On the contrary, the spectra of RE

ions in an amorphous matrix like a glass, present an inhomogeneous broadening due to the different sites occupied by the ions in the host and thus, different crystal fields. As a consequence the Stark structure of RE spectra in glasses is only partially resolved even at low temperature. On the other hand, the symmetry and strength of the CF also affect the splitting of the levels. Moreover, the probability of radiative and nonradiative transitions is strongly affected by the host matrix.

Among rare-earth ions, Nd^{3+} has been recognized as one of the most efficient RE ions for solid-state lasers in crystals and glasses due to its intense $^4F_{3/2} \rightarrow {}^4I_{11/2}$ emission at around 1.06 μm [19]. Besides the interest of Nd^{3+} ions in the field of IR optical amplification, this ion can also be used as a probe for local ordering due to the close relation between its spectroscopic properties and the local structure and bonding at the ion site [19, 20].

In this work, we show how steady-state and time-resolved site-selective laser spectroscopies allow to isolate unambiguously the emission of Nd^{3+} ions occupying La^{3+} sites in the LaF_3 nanocrystals precipitated in transparent oxyfluoride glass-ceramics obtained by the adequate heat treatment of a Nd^{3+}-doped glass with composition SiO_2-Al_2O_3-Na_2O-LaF_3, from that produced by the Nd^{3+} ions sitting in the glass matrix. A strong reduction of the lifetimes of Nd^{3+} in the crystalline phase is observed for concentrations higher than 0.1% and attributed to the much higher concentration of Nd^{3+} in nanocrystals with respect to glass matrices.

16.2 Structural Characterization

Glasses of composition $55SiO_2$–$20Al_2O_3$-$15Na_2O$-$10LaF_3$ doped with 0.1, 0.2, 0.5, 1 and 2 Nd^{3+} (in mol %) have been prepared by melting-quenching by using as raw materials: SiO_2 (Saint-Gobain, 99.6%), Al_2O_3 (Panreac), Na_2CO_3 (Sigma Aldrich, >99.5%), LaF_3 (Alfa Aesar, 99.9%), and NdF_3 (Alfa Aesar, 99.99%). The batches were calcined at 1200 °C for 2 h, melted at 1650 °C for 1.5 h, and then quenched onto a brass mould. Glasses were melted again for 30 min and quenched onto a cold (−10 °C) brass mould. All the glasses were annealed at 600 ° C for 30 min to eliminate residual stresses. From now on, glass samples will be labelled by G0.1, G0.2, G0.5, G1 and G2, for Nd^{3+} concentrations equal to 0.1, 0.2, 0.5, 1, and 2, respectively, while corresponding glass-ceramics will be denoted by GCx.

Glass-ceramic samples were obtained by heat treatments of glass pieces at 620 °C for 1, 3, 5, 20, 40, 80 h, 660 °C-20 h, and 680 °C-20 h using a heating rate of 10 °C/min [21]. Glass sheets (1 cm × 1 cm × 2 mm) were treated and then polished for optical characterization. One glass lamella for each composition was not treated and used as reference glass for comparison with the corresponding glass-ceramics. The heat-treated samples were milled, sieved (<63 μm) and characterised by XRD (Bruker D8 Advance). XRD diffractograms were acquired in the 10–70° range, with

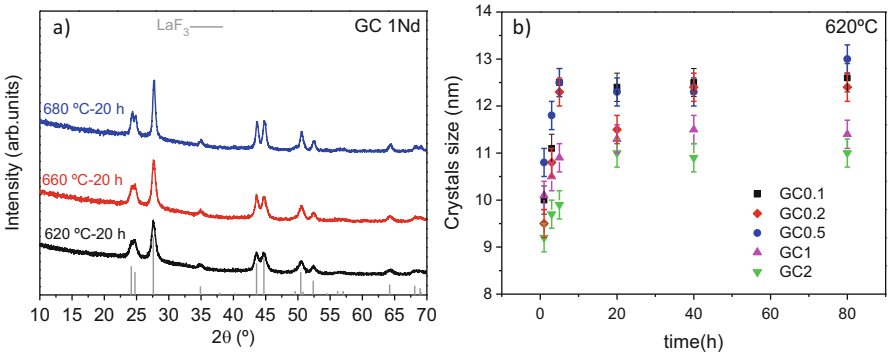

Fig. 16.1 (**a**) XRD diffractograms of GC1 samples heat treated at 620 °C-20 h, 660 °C-20 h, and 680-20 h. (**b**) Crystals size for the samples doped with different NdF_3 concentrations treated at 620 °C

0.02° step and 1 s acquisition for each step. The crystals size was calculated using the Scherrer equation [22]:

$$D = \frac{0.94\lambda}{\cos\,\theta\sqrt{B_m^2 - B_i^2}} \tag{16.1}$$

where λ is the wavelength (1.54056 Å – CuKα_1), B_m the FWHM of the LaF_3 peak (111) and θ its diffraction angle. Factor 0.94 corresponds to spherical crystals. Pseudo-Voigt function has been used to fit diffraction peak parameters. The instrumental broadening B_i has been also taken into account using NaF powder properly milled and sieved (<63 μm).

Figure 16.1a shows the XRD diffractograms of GC1 samples heat treated at 620 °C-20 h, 660 °C-20 h, and 680-20 h. On the bottom the LaF_3 peaks are given (JCPDS 00-032-0483) as reference. For all the compositions, only LaF_3 crystals precipitate in the glass matrix, but the crystal growth kinetics slows down as Nd^{3+} content increases. The inset shows the crystal size after 20 h of treatment at 620, 660, and 680 °C. Figure 16.1b shows the crystals size of GCs heat treated at 620 °C for all the Nd^{3+} concentrations. As can be seen the crystal size increases during the first 5 h reaching a constant value independent on the time of treatment. On the other hand as Nd^{3+} concentration increases the crystal size becomes smaller. LaF_3 nanocrystals grow from 10 nm to 12.5 nm during the first 5 h for the G0.1 glass, but grow less than 1 nm for G2 glass. This may be explained on consideration of the higher T_g of G2 glass. For 660 °C-20 h heat treatment bigger crystals are formed but a similar trend as for 620 °C is maintained [21].

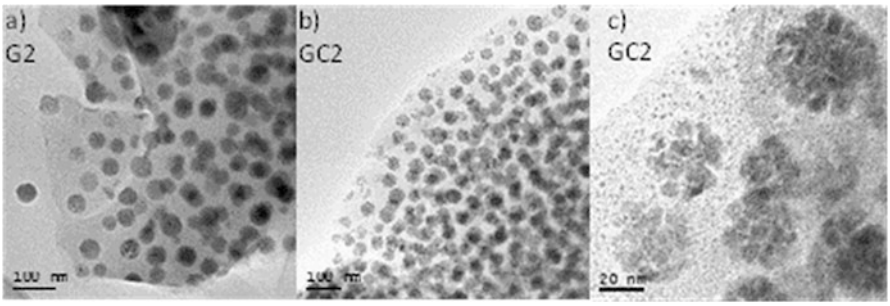

Fig. 16.2 HR-TEM of G2 glass (**a**) and GC2 heat treated at 620 °C-40 h (**b**) and (**c**)

TEM samples of glasses and glass-ceramics were prepared using sieved powders of size <63 μm. High resolution electron microscopy (HR-TEM), including Scanning Transmission Microscopy-High Angle Annular Dark Field (STEM-HAADF) and X-Ray Energy Dispersive Spectroscopy (EDXS), were recorded on a JEOL 2100 field emission gun transmission electron microscope, operating at 200 kV and providing a point resolution of 0.19 nm. The TEM is equipped with an EDXS energy dispersive X-ray spectrometer (INCA x-sight, Oxford Instruments). EDXS analysis was performed in STEM mode, with a probe size of 1 nm. TEM analysis clearly demonstrates the formation of nanocrystals in the heat treated samples. As an example, Fig. 16.2a shows the micrograph of the glass sample doped with 2 mol% of NdF_3 where phase separation droplets are observed. The main size of the droplets in the glass is around 35 nm.

The micrographs of the sample treated at 620 °C-40 h (Fig. 16.2b, c) show the formation of NCs inside the droplets. The main size of the droplets is similar to the glass sample and the average crystal size is around 10 nm in agreement with the values obtained from the diffractograms.

The incorporation of Nd^{3+} ions into the NCs has been demonstrated by Energy Dispersive X-ray (EDX) spectroscopy. As can be seen in Fig. 16.3, the crystallized droplets show an excess of La, F, and Nd, whereas Si is confined mostly at the interface between the droplets which leads to the formation of a barrier around them. The barrier formation should occur during the first 20 h of treatment since LaF_3 crystals grow up to this time, and constant values are stabilized for longer times. The yellow line is the scanning line. The incorporation of Nd^{3+} into crystals of LaF_3 is clearly visible from the EDX curves.

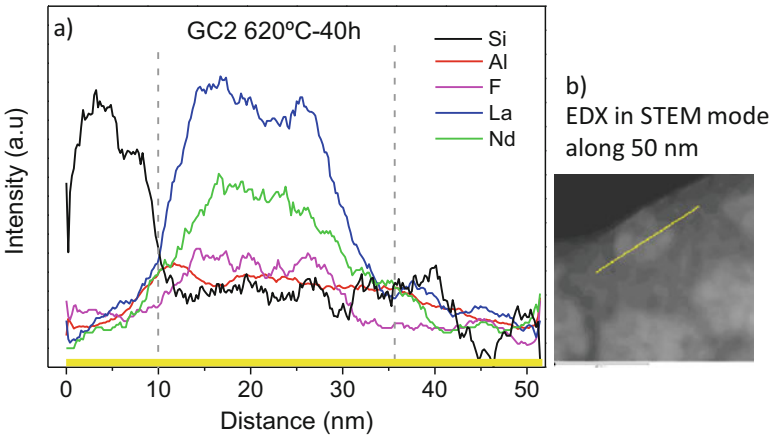

Fig. 16.3 (**a**) EDX of the GC2 620 °C-40 h sample. The yellow line indicates the scanning line. (**b**) STEM image of the droplets used for the EDX measurements. The yellow line represents the same as in (**a**)

16.3 Absorption and Emission Properties of Nd^{3+} Ions

16.3.1 Absorption Properties

Figure 16.4a shows the absorption coefficient for the glass and GC samples treated at 620 °C-20, 620 °C-40 h, and 660 °C-20 h doped with 2 mol% the bands observed in the spectra correspond to transitions from the fundamental level ($^4I_{9/2}$) to each of the excited levels of Nd^{3+} ions. The glass sample presents the characteristic inhomogeneously broadened absorption bands. However, in the case of the GC samples, better resolved absorption bands are observed indicating the incorporation of Nd^{3+} ions in the LaF_3 nanocrystals precipitated during the heat treatments. Figure 16.4b presents in more detail the absorption band of the hypersensitive transition and the bands around 750 and 800 nm for different glass and GC samples. As can be seen, in the case of the GC samples the bands present a more resolved structure and a reduction of the inhomogeneous broadening.

The absorption spectra have been used to calculate the radiative lifetime of the $^4F_{3/2}$ excited J manifold, the branching ratios, and the radiative transition probabilities of fluorescence transitions to the lower lying ^4I_J manifolds, according to the Judd-Ofelt (JO) theory [23, 24]. The experimental oscillator strengths of the absorption bands originating from the $^4I_{9/2}$ ground state have been calculated for the samples doped with 2 mol% by using the expression:

$$f_{\exp} = \frac{mc}{\pi e^2 N} \int_{band} \alpha(\nu) d\nu \tag{16.2}$$

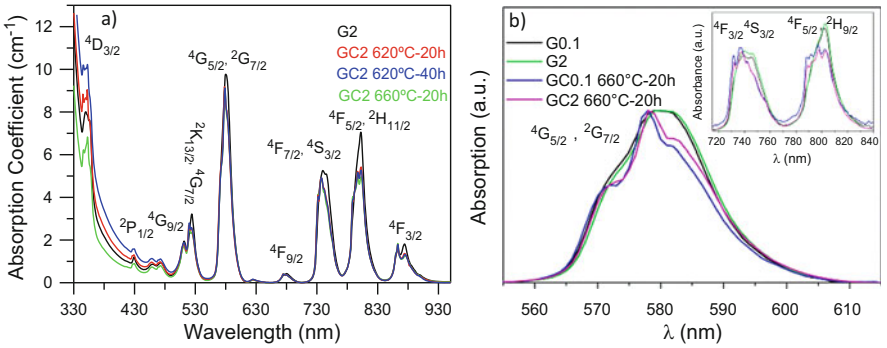

Fig. 16.4 (**a**) Absorption coefficient for the glass and GC samples doped with 2 mol% of NdF_3. (**b**) Enlarged views of absorption bands corresponding to the $^4I_{9/2} \rightarrow {}^4G_{5/2}$, $^2G_{7/2}$ and (inset) $^4I_{9/2} \rightarrow {}^4F_{7/2}$, $^4S_{3/2}$ and $^4I_{9/2} \rightarrow {}^4F_{5/2}$, $^2H_{9/2}$ for G0.1, G0.2, GC01, and GC2

where m and e are the electron mass and charge respectively, c is the light velocity, N is the number of ions per unit volume, and $\alpha(\nu)$ is the absorption coefficient. The experimental f values have been used to calculate the Ω_t parameters corresponding to the JO theory. In the framework of this theory the radiative electric-dipole transitions within the $4f^n$ configuration from the initial state |a J>, to the final state |b J′ > can be described in terms of the oscillator strength by using:

$$f_{cal}\left(aJ;bJ'\right) = \frac{8\pi^2 m\nu}{3h\left(2J+1\right)e^2 n^2}\left[\chi_{ed} S_{ed}\left(aJ;bJ'\right)\right] \tag{16.3}$$

where m is the mass of the electron, ν is the frequency of the transition, h the Planck's constant, J is the total angular momentum of the initial state (J = 9/2 in Nd^{3+}), e the electron charge, and n is the refractive index of the host $\chi_{ed} = [n(n^2 + 2)^2]/9$ is the effective field correction at a well-localized center in a medium of refractive index n. S_{ed} is the line strength for electric-dipole transitions expressed by:

$$S_{ed} = e^2 \sum_{t=2,4,6} \Omega_t \left|\left\langle aJ \left\| U^{(t)} \right\| bJ' \right\rangle\right|^2 \tag{16.4}$$

where $<|| U^{(t)} ||>$ are the double-reduced matrix elements of the unit tensor operators which are considered to be independent of the host matrix and Ω_t are the JO parameters. We have used the values reported by Carnall et al. for Nd^{3+} ions in LaF_3 [25]. The best set of Ω_t parameters can be determined by a least-squared fitting of the calculated and experimental oscillator strengths. The JO parameters obtained from the fitting are displayed in Table 16.1 for the glass and glass-ceramic samples doped with 2 mol% of NdF_3. The values of the root mean square (r.m.s.) indicate a good agreement between the experimental and calculated oscillator strengths.

Table 16.1 Judd-Ofelt parameters and r.m.s. deviation for glass and glass-ceramic samples doped with 2 mol% NdF_3

Sample	Ω_2 ($\times 10^{-20}$)	Ω_4 ($\times 10^{-20}$)	Ω_6 ($\times 10^{-20}$)	r.m.s.
Glass	3.23	6.23	5.03	5.35×10^{-7}
GC2–620 °C-20 h	2.85	5.57	4.37	5.25×10^{-7}
GC2–620 °C-40 h	2.82	5.48	4.31	5.16×10^{-7}
GC2–660 °C-20 h	2.89	5.45	4.17	5.35×10^{-7}

The value of Ω_2 in the GC samples is lower than in the glass sample, which means that the heat treatment induces a reduction in the degree of covalency in the rare-earth site. It is well known that Ω_2 is most sensitive to local structure and its value is indicative of the amount of covalent bonding between RE ions and ligand anions [26]. The decrease of Ω_2 further confirms the incorporation of Nd^{3+} ions into the fluoride NCs. Moreover, the sum of the JO parameters decreases for the GC sample due to the decrease of covalency of the chemical bond between the Er^{3+} ion and the ligand anions [27]. This is in accordance with reported results that predict that the sum decreases in the oxide > oxyfluoride > fluoride sequence. In addition, the Ω_2 parameter is closely related to the hypersensitive transitions. The more intense the hypersensitive transition is, the larger the Ω_2 value. The oscillator strength of this transition is reduced from 1796×10^{-8} in the glass to 1609×10^{-8}, 1581×10^{-8}, and 1591×10^{-8} in the GC 620 °C C-20 h, GC 620 °C-40 h, and GC 660 °C-20 h samples respectively, which confirms that the ligand field around Nd^{3+} ions has changed as a consequence of the heat treatment and crystallisation process.

The spontaneous emission probabilities from the $^4F_{3/2}$ level to the $^4I_{15/2,\ 13/2,\ 11/2,\ 9/2}$ ones can be calculated from the JO parameters. The radiative transition probability from the initial J to the terminal J′ manifold is given by:

$$A\left(aJ; bJ'\right) = \frac{64\pi^4 \nu^3}{3h\left(2J+1\right)c^3}\left[n\frac{\left(n^2+2\right)^2}{9}S_{ed}\right] \tag{16.5}$$

where n is the refractive index, ν is the frequency of the transition and J' is the terminal manifold.

The radiative lifetime of an emitting level is related to the total spontaneous emission probability from this level by:

$$\tau_R = \left\{\sum_{bJ'} A\left(aJ; bJ'\right)\right\}^{-1} \tag{16.6}$$

The emission branching ratio can be obtained from the transition probabilities by using:

$$\beta = \frac{A\left(aJ; bJ'\right)}{\sum\limits_{bJ'} A\left(aJ; bJ'\right)} \tag{16.7}$$

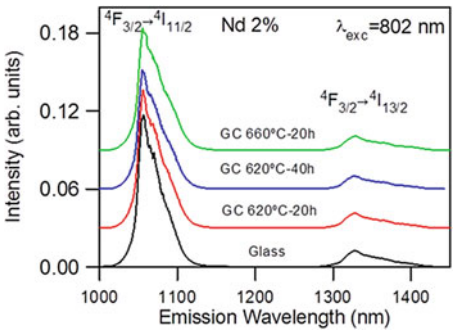

Fig. 16.5 Room temperature emission spectra for the glass and GC samples doped with 2 mol% of NdF_3

16.3.2 Fluorescence Properties

The $^4F_{3/2}\rightarrow^4I_{11/2,13/2}$ steady-state fluorescence spectra were measured at room temperature for all samples by exciting with a Ti-sapphire laser at 802 nm in resonance with the $^4I_{9/2}\rightarrow^4F_{5/2},^2H_{9/2}$ absorption band. The fluorescence was analyzed with a 0.25 monochromator, and the signal was detected by a Hamamatsu H10330A-75 photomultiplier and finally amplified by a standard lock-in technique. As an example, Fig. 16.5 shows the emission for the samples doped with 2 mol%. As can be seen in this figure, the emission is inhomogeneously broadened due to site-to-site variations in the local ligand field. Since the $^4F_{3/2}\rightarrow^4I_{11/2}$ emission band is slightly asymmetric an effective linewidth was determined by integrating the fluorescnce lineshape and dividing by the intensity at the peak fluorescence emission wavelength. The stimulated emission cross-section can be determined from spectral parameters using [28],

$$\sigma_p\left(\lambda_p\right) = \frac{\lambda_p^4}{8\pi cn^2\Delta\lambda_{eff}} A\left[\left(^4F_{3/2}\right);\left(^4I_{11/2}\right)\right] \tag{16.8}$$

where λ_p is the peak fluorescence wavelength, n is the refractive index, $\Delta\lambda_{eff}$ is the effective linewidth of the $^4F_{3/2}\rightarrow^4I_{11/2}$ transition, and $A[(^4F_{3/2});(^4I_{11/2})]$ is the radiative transition probability for this transition.

The stimulated emission cross-section for the $^4F_{3/2}\rightarrow^4I_{11/2}$ transition is presented in Table 16.2 together with the effective fluorescence linewidth ($\Delta\lambda_{eff}$), refractive index (n), and peak position (λ_p). The peak position remains unchanged for the GC samples and the effective linewidth slightly increases with the heat treatment. This, together with the lower radiative transition probability for the $^4F_{3/2}\rightarrow^4I_{11/2}$ emission for the heat treated samples, leads to smaller stimulated

Table 16.2 Room temperature emission properties of Nd^{3+} (2 mol%) in the glass and glass-ceramic samples

Sample	n	λ_p(nm)	$\Delta\lambda_{eff}$ (nm)	σ_p (pm^2)
Glass	1.523	1057	35.95	2.8
GC2–620 °C-20 h	1.525	1057	37.16	2.4
GC2–620 °C-40 h	1.526	1057	37.60	2.3
GC2–660 °C-20 h	1.526	1057	38.94	2.2

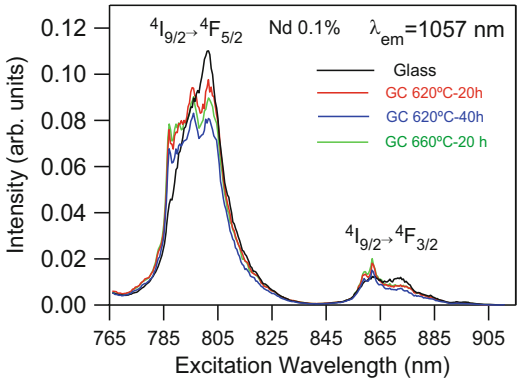

Fig. 16.6 Room temperature excitation spectra for the glass and GC samples doped with 0.1 mol% of NdF_3

emission cross-sections for the GC samples. The stimulated emission cross-section in these samples is in the range of the values found in silicate glasses (0.9–3.6 pm^2) [19].

The steady-state emission spectra present similar spectral features for all concentrations and heat treatments; however the excitation spectra of the GC samples doped with 0.1 0.2, and, 0.5 mol% performed in the 765–905 nm spectral range monitored at 1057 nm show, superimposed to the broad $^4I_{9/2}\rightarrow{}^4F_{5/2,3/2}$ bands of the glass, a fine structure which confirms the partial incorporation of Nd^{3+} ions in the NCs. As we shall see in the next section in the samples doped with 1 and 2 mol% the main contribution to the spectra belong to the Nd^{3+} ions in the amorphous environment. As an example Fig. 16.6 shows the excitation spectrum for the samples doped with 0.1 mol% of NdF_3.

16.3.3 Lifetime Results

The decays of the $^4F_{3/2}$ state were obtained by exciting with a pulsed Ti-sapphire laser at 802 nm in the $^4I_{9/2}\rightarrow{}^4F_{5/2}$ absorption band at 295 K by using a Ti-sapphire laser pumped by a pulsed frequency doubled Nd:YAG laser (9 ns pulse width). The decays of the samples doped with 0.1 and 0.2 mol% can be described to a good approximation by a single exponential function whereas the decays of the samples

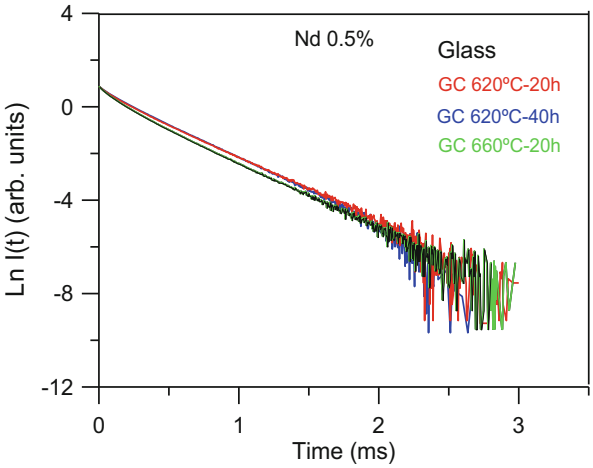

Fig. 16.7 Semilogarithmic plot of the room temperature experimental decays from the $^4F_{3/2}$ state for the samples doped with 0.5 mol% of NdF_3. The decays were obtained by exciting at the $^4I_{9/2} \rightarrow {}^4F_{5/2}$ transition and monitored at 1057 nm

Table 16.3 Experimental lifetimes of the $^4F_{3/2}$ level obtained under excitation at 802 nm collecting the luminescence at 1057 nm as a function of Nd^{3+} concentration and heat treatment

Sample	0.1%	0.2%	0.5%	1%	2%	τ_R (μs)
Glass	343	298	268	192	143	345
GC2–620 °C-20 h	382	350	308	251	187	390
GC2–620 °C-40 h	385	354	310	254	191	395
GC2–660 °C-20 h	388	359	315	254	197	398

The radiative lifetime is shown in the last column

with higher Nd^{3+} concentrations deviate from a single exponential and the lifetime decreases. As an example, Fig. 16.7 shows the logarithmic plot of the experimental decays of the $^4F_{3/2}$ level for the sample doped with 0.5 mol% of NdF_3 at room temperature. Table 16.3 displays the lifetime values for all samples. The lifetime value for the samples with concentrations higher than 0.1 mol% corresponds to the average lifetime defined by

$$\langle \tau \rangle \frac{\int I(t)dt}{I_0}$$

where I(t) is the intensity at time t. According to the value of the radiative lifetime the quantum efficiencies ($\eta = \tau_{exp}/\tau_R$) are around 99 and 41% for the glass samples doped with 0.1 and 2 mol% respectively. This reduction of the quantum efficiency as concentration increases indicates the presence of non-radiative cross-relaxation processes such as ($^4F_{3/2}$, $^4I_{9/2}$)→ ($^4I_{15/2}$, $^4I_{15/2}$).

The lifetime of the GC samples is longer than the lifetime of the glass samples for all concentrations which suggests a fluoride environment for Nd^{3+} ions according with their incorporation in the nanocrystalline phase.

The lifetime of an emitting level is governed by a sum of probabilities of several competing processes: radiative decay, nonradiative decay by multiphonon relaxation and by energy transfer to other ions.

$$\frac{1}{\tau_{\exp}} = \frac{1}{\tau_R} + W_{NR} = \frac{1}{\tau_R} + W_{MPH} + W_{ET} \tag{16.9}$$

where W_{NR} is the nonradiative probability. This nonradiative probability can be due to multiphonon relaxation, which depends on the host matrix, and/or energy transfer which is dependent on ion concentration. Nonradiative decay by multiphonon emission is expected to be small in this case because the energy difference between $^4F_{3/2}$ and $^4I_{15/2}$ levels is around 5500 cm^{-1} and the highest phonon energy is about 1000 cm^{-1}. This corresponds to more than 5 phonons, which indicates that the multiphonon relaxation process is weak and can be neglected in this case. Hence at low concentration (0.1%) the experimental lifetime, which is single exponential, should approach the radiative lifetime. As the concentration rises, the lifetime decreases, which indicates that Nd-Nd relaxation processes such as ($^4F_{3/2} \rightarrow {}^4I_{15/2}$) ($^4F_{3/2} \rightarrow {}^4I_{11/2}$) processes in which two ions exchange energy, play an important role [29].

16.4 Site-Selective Spectroscopy

The $^4F_{3/2} \rightarrow {}^4I_{11/2}$ transition of Nd^{3+} ions can show variations in peak wavelength, linewidth, and spectral profile depending on pumping wavelength due to the site-to-site variation of the local field acting on the ions. To obtain further information about the different environments for Nd^{3+} ions in these glass-ceramics, we have performed site-selective spectroscopy by using a Ti-sapphire ring laser with a narrow bandwidth (0.08 cm^{-1}) as an excitation source for the $^4I_{9/2} \rightarrow {}^4F_{5/2}$ transition. Figure 16.8a shows the normalized emission spectra obtained by exciting at 786 and 802 nm for the GC sample doped with 0.2 mol% of NdF_3 treated at 620 °C-40 h. As can be observed in this figure the shape, peak position, and linewidth of the emission band change depending on the excitation wavelength, which indicates that Nd^{3+} ions are in different crystal field sites. The spectrum obtained by exciting at 786 nm shows a more resolved structure which indicates a crystalline environment for Nd^{3+} ions, whereas the one obtained under excitation at 802 nm shows the inhomogeneous broadened band similar to the glass sample. Moreover, the excitation spectra obtained by collecting the luminescence at 1039 and 1057 nm also show the presence of different environments for Nd^{3+} ions. Figure 16.8b shows the normalized excitation spectra for the same GC sample doped with 0.2 mol% of NdF_3. The spectrum monitored at 1039 nm presents narrower and well-resolved peaks corresponding to Nd^{3+} ions in the NCs. As concentration increases the spectra become broader and less resolved. Similar results are obtained for the three heat treatments, which indicates that after a 20 h treatment at 620 °C the Nd^{3+} ions are incorporated in the NCs.

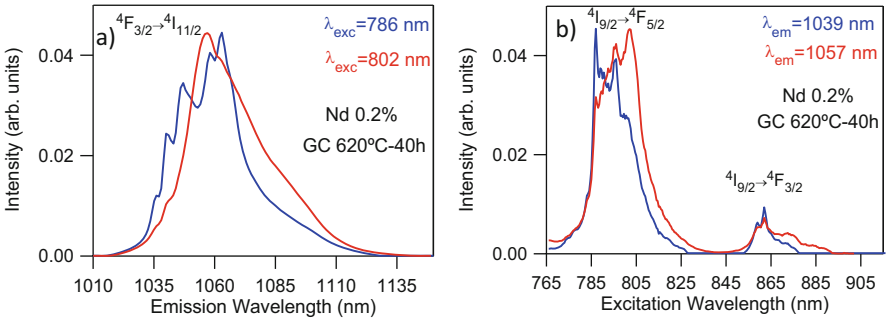

Fig. 16.8 (**a**) Room temperature normalized emission spectra obtained under excitation at 786 (blue) and 802 (red) nm for the GC treated at 620 °C-40 h sample doped with 0.2 mol% of NdF_3. (**b**) Normalized excitation spectra obtained by collecting the luminescence at 1039 and 1057 nm for the GC treated at 620 °C-40 h sample doped with 0.2 mol% of NdF_3

To clearly identify the emission from the Nd^{3+} ions in the NCs, the emission and excitation spectra have been measured at low temperature, in order to minimize the overlapping of the contributions from Nd^{3+} in the crystalline and amorphous phases due to the thermal population of the higher energy Stark components of the ground and excited states. The low temperature (9 K) excitation spectra are presented in Fig. 16.9 for the GC samples doped with 0.2 and 1 mol% treated at 620 °C-40 h. As observed in the spectra obtained at 1039 nm, the low energy band corresponding to the $^4I_{9/2}\rightarrow{}^4F_{3/2}$ doublet narrows and defines into two single components as expected for a well defined crystal field site. Moreover, the $^4I_{9/2}\rightarrow{}^4F_{5/2}$ band is composed of narrow and well resolved peaks which indicate that the spectra obtained at 1039 nm correspond to Nd^{3+} ions in the LaF_3 nanocrystals whereas the spectra obtained at 1055 nm show broad bands similar to those found in the glass samples. On the other side, the relative intensity of the contributions from Nd^{3+} ions in the NCs and in the amorphous matrix changes as Nd^{3+} concentration increases. At low concentrations, the higher intensity corresponds to Nd^{3+} in the crystalline phase.

In order to confirm if the features shown by the excitation spectra monitored at 1039 nm can be definitely related to the Nd^{3+} ions in the NCs, site-selective steady-state, emission spectra for the $^4F_{3/2}\rightarrow{}^4I_{11/2}$ transition were recorded by exciting at 786 and 802 nm. Figure 16.10 shows the emission spectra at 9 K obtained under excitation at 786 and 802 nm for the GC samples doped with 0.2 and 1 mol%. Different spectral features are observed depending on the excitation wavelength. The spectrum obtained under excitation at 786 nm shows sharp peaks, one at 1039 nm not overlapping with the emission spectrum obtained by exciting at 802 nm. This spectrum corresponds to the one obtained in pure LaF_3 crystals [30, 31]. The sharp peaks disappear and the spectrum becomes broader and similar to that found in the glass sample for 802 nm excitation. These results indicate that at 786 nm Nd^{3+} ions in the crystalline phase are excited. As concentration increases,

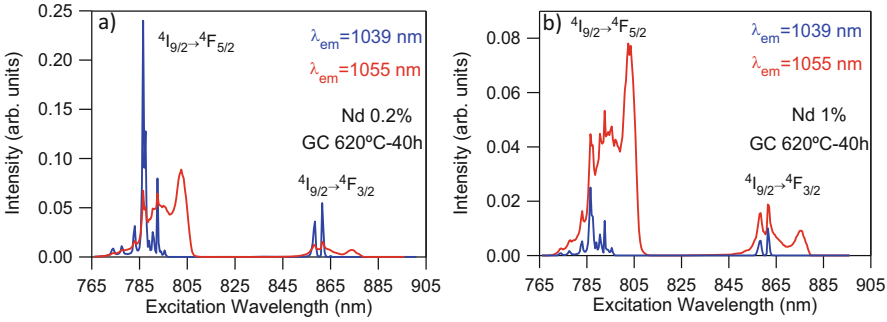

Fig. 16.9 Low temperature excitation spectra obtained by collecting the luminescence at 1039 (blue) and 1055 nm (red) for the GC samples doped with (**a**) 0.2 and (**b**) 1 mol% of NdF_3

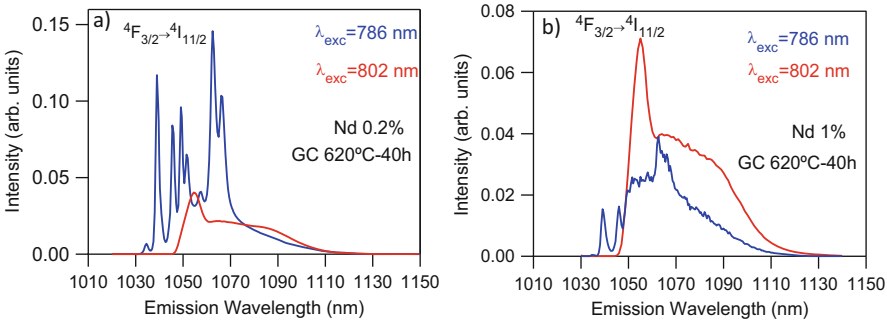

Fig. 16.10 Low temperature emission spectra obtained under excitation at 786 (blue) and 802 nm (red) for the GC samples doped with (**a**) 0.2 and (**b**) 1 mol% of NdF_3

the emission from Nd^{3+} ions in the NCs decreases and the spectra become broader and with less resolved peaks. Similar emission spectra are obtained by exciting the $^4I_{9/2}\rightarrow{}^4F_{3/2}$ band at 861.5 and 876 nm.

Furthermore, the existence of different environments for Nd^{3+} ions is also reflected by the lifetimes of the $^4F_{3/2}$ state. Lifetime measurements of the $^4F_{3/2}$ state were performed by exciting the samples at 786 and 802 nm by using a Ti-sapphire laser pumped by a pulsed frequency doubled Nd:YAG laser (9 ns pulse width), and collecting the luminescence at 1039 and 1055 nm respectively. If Nd^{3+} ions are incorporated in the LaF_3 NCs, the lifetime values should depend on the excitation and emission wavelengths. Under excitation at 786 nm and collecting the luminescence at 1039 nm the decay is single exponential with a lifetime of 688 μs for the GC sample doped with 0.1% whereas by exciting at 802 nm and collecting the luminescence at 1055 nm the lifetime is 336 μs. The longer lifetime corresponds to the Nd^{3+} ions incorporated in the NCs. Table 16.4 shows the lifetime values as a function of Nd^{3+} concentration for the GC samples treated at 620 °C-40 h. As can be seen, the Nd^{3+} lifetime in the crystalline phase is strongly reduced as concentration increases being 98 μs for the GC sample doped with 1 mol%.

Table 16.4 Experimental lifetimes, at low temperature, of the $^4F_{3/2}$ level obtained under excitation at 786 and 802 nm collecting the luminescence at 1039 and 1055 nm respectively

%NdF_3	λ_{exc} = 786 nm	λ_{exc} = 802 nm
	τ_{exp} (μs)	τ_{exp} (μs)
0.1	688	336
0.2	462	337
0.5	188	332
1	98	295

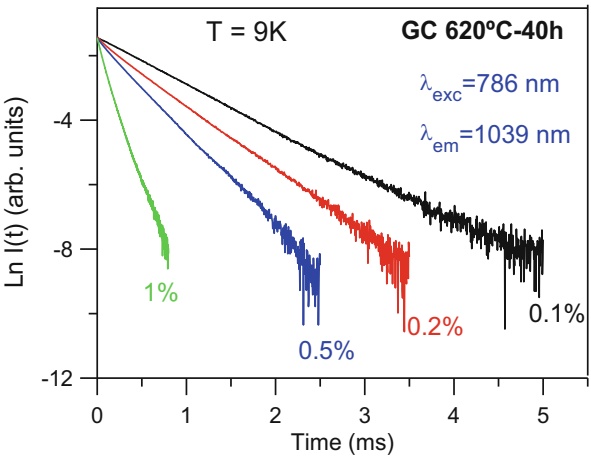

Fig. 16.11 Semi-logarithmic plot of the experimental decays from the $^4F_{3/2}$ state obtained under excitation at 786 nm collecting the luminescence at 1039 nm for the GC samples doped with 0.1, 0.2, 0.5, and 1 mol% of NdF_3

Figure 16.11 shows the semi-logarithmic plot of the experimental decays of the $^4F_{3/2}$ level for the samples doped with 0.1, 0.2, 0.5, and 1 mol% of NdF_3 under selective excitation (786 nm) and emission (1039 nm) wavelengths at which it is possible to separate the Nd^{3+} contribution in the crystalline phase.

As can be observed in Table 16.4 and Fig. 16.11 there is a strong quenching of the Nd^{3+} lifetimes in the LaF_3 nanocrystals, being much less relevant in the amorphous phase. This behaviour is likely explained by a high diffusion of Nd^{3+} ions from the glass matrix to the LaF_3 nanocrystals, as confirmed in the same system doped with Tm^{3+} studied by XANES with Synchrotron radiation [32].

16.5 Conclusions

Transparent oxyfluoride nano-glass-ceramics containing LaF_3 crystals with a crystal size between 9–13 nm have been obtained after proper heat treatments at T_g + 20–80 °C as confirmed by X-ray diffraction (XRD) and high resolution transmission electron microscopy (HR-TEM). A detailed optical characterization clearly shows that Nd^{3+} ions in glass-ceramics are incorporated in both crystalline and amorphous phases. The low temperature site-selective emission and excitation spectra, together with the different lifetime values of the $^4F_{3/2}$ state depending on the excitation

and emission wavelengths, allow to isolate unambiguously the emission from Nd^{3+} ions in the LaF_3 nanocrystals and to correlate the spectroscopic properties with the structural properties. As the Nd^{3+} concentration is increased beyond 0.1 mol%, a stronger quenching of lifetime is observed for Nd^{3+} ions inside LaF_3 crystals than for those dispersed in the glass matrix. This strong concentration quenching is explained by the much higher concentration of Nd^{3+} ions in the crystalline phase compared to the one in the glass matrix.

Acknowledgments This work was supported by the Spanish Government MEC under Projects MAT2013-48246-C2-2-P and MAT2013-48246-C2-1-P and the University of the Basque Country PPG17/07.

References

1. Blasse G, Grabmaier BC (1994) Luminescent materials. Springer, New York
2. Downing E, Hesselink L, Ralston J, Macfarlane R (1996) A three-color, solid-state, three-dimensional display. Science 273:1185–1189
3. Desurvire E (1994) Erbium-doped fiber amplifiers: principles and applications. Wiley, New York
4. Wang F, Han Y, Lim CS, Lu Y, Wang J, Xu J, Chen H, Zhang C, Hong M, Liu X (2010) Simultaneous phase and size control of upconversion nanocrystals through lanthanide doping. Nature 463:1061–1065
5. Huang X, Han S, Huang W, Liu X (2013) Enhancing solar cell efficiency: the search for luminescent materials as spectral converters. Chem Soc Rev 42:173–201
6. de Pablos-Martin A, Ferrari M, Pascual MJ, Righini GC (2015) Glass-ceramics: a class of nanostructured materials for photonics. Rivista del Nuovo Cimento 38:311–369
7. Fedorov PP, Luginina AA, Popov AI (2015) Transparent oxyfluoride glass ceramics. J Fluor Chem 172:22–50
8. Wang Y, Ohwaki J (1993) New transparent vitroceramics codoped with Er^{3+} and Yb^{3+} for efficient frequency upconversion. J. App Phys Lett 63:3268–3270
9. Chen D, Yu Y, Huang P, Lin H, Shan Z, Wang Y (2010) Color-tunable luminescence of Eu^{3+} in LaF_3 embedded nanocomposite for light emitting diode. Acta Mater 58:3035–3041
10. Luo Q, Qiao X, Fan X, Yang H, Zhang X, Cui S, Wang L, Wang G (2009) Luminescence behavior of Ce^{3+} and Dy^{3+} codoped oxyfluoride glasses and glass ceramics containing LaF_3 nanocrystals. J Appl Phys 105:043506
11. Velazquez JJ, Rodriguez VD, Yanes AC, del-Castillo J, Mendez-Ramos J (2010) Increase in the Tb^{3+} green emission in SiO_2-LaF_3 nano-glass-ceramics by codoping with Dy^{3+} ions. J Appl Phys 108:113530
12. Secu M, Secu CE, Polosan S, Aldica G, Chica C (2009) Crystallization and spectroscopic properties of Eu-doped CaF_2 nanocrystals in transparent oxyfluoride glass-ceramics. J Non-Cryst Solids 355:1869–1872
13. Sun X, Gu M, Huang S, Jin X, Lui X, Liu B, Ni C (2009) Luminescence behavior of Tb^{3+} ions in transparent glass and glass-ceramics containing CaF_2 nanocrystals. J Lumin 129:773–777
14. Qiao X, Fan X, Wang M (2006) Luminescence behavior of Er^{3+} in glass ceramics containing BaF_2 nanocrystals. Scripta Mater 55:211–216
15. Luo Q, Fan X, Qiao X, Yang H, Wang M, Zhang X (2009) Eu^{2+}-doped glass ceramics containing BaF_2 nanocrystals as a potential blue phosphor for UV-LED. J Am Ceram Soc 92:942–944

16. Goncalves MC, Santos LF, Almeida RM (2002) Rare-earth-doped transparent glass ceramics. CR Chimie 5:845–854
17. de Pablos-Martín A, Durán A, Pascual MJ (2012) Nanocrystallisation in oxyfluoride systems: mechanisms of crystallisation and photonic properties. Int Mater Rev 57:165–186
18. Russell HN, Saunders FA (1925) New regularities in the spectra of the alkaline earths. Astrophys J 61:38–69
19. Weber MJ (1990) Science and technology of laser glass. J Non-Cryst Solids 123:208–222
20. Jacobs RR, Weber MJ (1976) Dependence of the $^4F_{3/2} \rightarrow {}^4I_{11/2}$ induced-emission cross section for Nd^{3+} on glass composition. IEEE J Quantum Electron QE-12:102–111
21. Gorni G, Velázquez JJ, Mather GC, Durán A, Chen G, Sundararajan M, Balda R, Fernández J, Pascual MJ (2017) Selective excitation in transparent oxyfluoride glass-ceramics doped with Nd^{3+}. J Eur Ceram Soc 37:1695–1706
22. Cullity D (1978) Elements of X-ray diffraction. Addison-Wesley, Reading
23. Judd BR (1962) Optical absorption intensities of rare-earth ions. Phys Rev 127:750–761
24. Ofelt GS (1962) Intensities of crystal spectra of rare-earth ions. J Chem Phys 37:511–520
25. Carnall WT, Crosswhite H, Crosswhite HM (1977) Energy level structure and transition probabilities of the trivalent lanthanides in LaF_3. Argonne National Laboratory, Argonne
26. Nachimuthu P, Jagannathan R (1999) Judd-Ofelt parameters, hypersensitivity, and emission characteristics of Ln^{3+} (Nd^{3+}, Ho^{3+}, and Er^{3+}) ions doped in PbO-PbF_2 glasses. J Am Soc 82(2):387–392
27. Mason SF, Peacock RD, Stewart B (1975) Ligand-polarization contributions to the intensity of hypersensitive trivalent lanthanide transitions. Mol Phys 30:1829–1841
28. Krupke WF (1974) Induced emission cross-sections in neodymium laser glasses. IEEE J Quantum Electron QE-10:450–457
29. Erhmann PR, Campell JH (2002) Nonradiative energy losses and radiation trapping in neodymium-doped phosphate laser glasses. J Am Ceram Soc 85:1061–1069
30. Dmitruk MV, Kaminskii AA (1968) Stimulated emission from LaF_3-Nd^{3+} crystal lasers. Sov Phys JET 26(3):531–533
31. Hong JQ, Zhang LH, Zhang PX, Wang YQ, Hang Y (2015) Growth, optical characterization and evaluation of laser properties of Nd: LaF_3 crystal. J Alloy Comp 646:706–709
32. de Pablos-Martín A, García MA, Muñoz-Noval A, Castro GR, Pascual MJ, Durán A (2014) Analysis of the distribution of Tm^{3+} ions in LaF_3 containing transparent glass-ceramics through X-ray absorption spectroscopy. J Non-Cryst Solids 384:83–87